The interplay of structural pathway and weathering intensity in forming mass-wasting processes in deeply weathered gneissic rocks (Sila Massif, Calabria, Italy)

Deborah Biondino, Luigi Borrelli, Salvatore Critelli, Francesco Muto & Giovanni Gullà

View supplementary material

Submit your article to this journal

View related articles

View Crossmark data

Science

🔓 OPEN ACCESS | Check for updates

The interplay of structural pathway and weathering intensity in forming mass-wasting processes in deeply weathered gneissic rocks (Sila Massif, Calabria, Italy)

Deborah Biondino[a], Luigi Borrelli [b], Salvatore Critelli[a], Francesco Muto[a] and Giovanni Gullà [b]

[a]Department of Biology, Ecology and Earth Sciences (DIBEST), University of Calabria, Rende, Italy; [b]National Research Council of Italy – Research Institute for geo-hydrological protection (CNR-IRPI), Rende, Italy

ABSTRACT

This paper presents a detailed map (Main Map) showing geology, tectonics, weathering intensity and spatial distribution of landslides in the San Pietro in Guarano study area (about 7.5 km^2), located in the north-western sector of Calabria (southern Italy). In this area, deeply weathered high-grade metamorphic rocks and different types/categories of mass movements are widespread. The Main Map, at 1:5000 scale, results from the combination of information gathered via analysis and interpretation of aerial photographs at different times and scales, multi-temporal geostructural and geomorphological surveys, field investigations and mapping of weathering grade in outcrop – through observation of geologically distinctive characteristics and qualitative and semi-quantitative engineering geological tests – integrated by means of the analysis of both weathering profiles on cutslopes and boreholes logs. The Main Map can represent a useful tool for authorities in charge of land-use planning and can profitably concur to typify landslides and to assess quantitative landslide risk.

1. Introduction

In geological contexts where high-grade metamorphic rocks outcrop, morphodynamic evolution of slopes and slope instability is strongly related to intensity and features of weathering profiles (Chigira & Ito, 1999; Matano & Di Nocera, 1999; Regmi, Yoshida, Dhital, & Pradhan, 2014; Whalley & Turkington, 2001). Since the weathering grade of crystalline rocks reflects their physical properties (Cascini & Gullà, 1993; Chiu & Charles, 2014; Gullà, Aceto, & Borrelli, 2012), in the study of weathering-related shallow, medium-deep and deep-seated landslides (e.g. Gullà, Peduto, Borrelli, Antronico, & Fornaro, 2017) is necessary to focus on the production of a specific geo-engineering map (the weathering grade map) based on multidisciplinary research which take into account geological, structural, geomorphological and some engineering geological aspects.

Classification and mapping of the weathering grade in outcrop (i.e. weathering grade field survey) are carried out through observation of geologically distinctive characteristics and several engineering geological tests (Borrelli, Coniglio, Critelli, La Barbera, & Gullà, 2015; Borrelli, Critelli, Gullà, and Muto, 2015; Cascini, Critelli, Di Nocera, Gullà, & Matano, 1992a; Matano & Di Nocera, 1999). In engineering geological studies

on weathered rocks (e.g. Calcaterra & Parise, 2010), a useful contribution to the weathering grade field survey is represented by an integrated analysis between weathering profiles on cutslopes (Borrelli, Greco, & Gullà, 2007; Gullà & Matano, 1997) and depth data derived from borehole logs (e.g. Borrelli & Gullà, 2017; Cascini, et al., 1992a). This analysis allows one to define the typical features of weathering profiles developed over crystalline rocks and to delineate characteristics and causes of their proneness to landsliding (Borrelli et al., 2007; Calcaterra & Parise, 2010; Cascini et al., 1992a, 1992b, 1994; Cascini & Gullà, 1993; Critelli, Di Nocera, & Le Pera, 1991; Gullà, Borrelli, & Greco, 2004).

This aspect can be considered relevant in Calabria (southern Italy), where weathered rocks are widespread and involved by landslides (Borrelli, Ciurleo, & Gullà, 2018; Calcaterra & Parise, 2005, 2010; Cascini et al., 1992a, 2017; Ciurleo, Cascini, & Calvello, 2017; Ietto, Perri, & Cella, 2018; Pellegrino & Prestininzi, 2007).

Indeed, the main mountain belts of Calabria are characterized by the extensive presence of weathered crystalline rocks (i.e. medium-to-high-grade metamorphic and plutonic rocks) that show moderate-to-deep weathering profiles (Borrelli, Perri, Critelli, & Gullà, 2012, 2014; Critelli et al., 1991; Guzzetta,

1974; Le Pera & Sorriso-Valvo, 2000; Le Pera, Critelli, & Sorriso-Valvo, 2001; Scarciglia, Le Pera, & Critelli, 2005, 2016).

In this context, the paper presents a detailed thematic map (Main Map) of the San Pietro in Guarano study area, about 7.5 km² (Figure 1), located in the north-western sector of Calabria (southern Italy). The study area, ranging in elevation from 350 to 1050 m a.s.l., presents a very complex morphology conditioned by lithologic characteristics, Quaternary tectonics and weathering processes.

The Main Map, showing the spatial distribution of geology, tectonics, weathering and landslides, has

been drawn using the data available for the study area (e.g. Cascini et al., 1992a, 1992b, 1994; Matano & Di Nocera, 1999; Matano & Tansi, 1994) integrated with detailed *in situ* surveys and investigations. The overall data analyses enable us to propose three simple block-models, which summarize the relationships between landslide categories and weathering profiles.

2. Geological setting of the Sila Massif

The San Pietro in Guarano area is located on the western border of the Sila Massif (Figure 1(A,B)), which represents part of a Hercynian orogenic belt (Calabrian
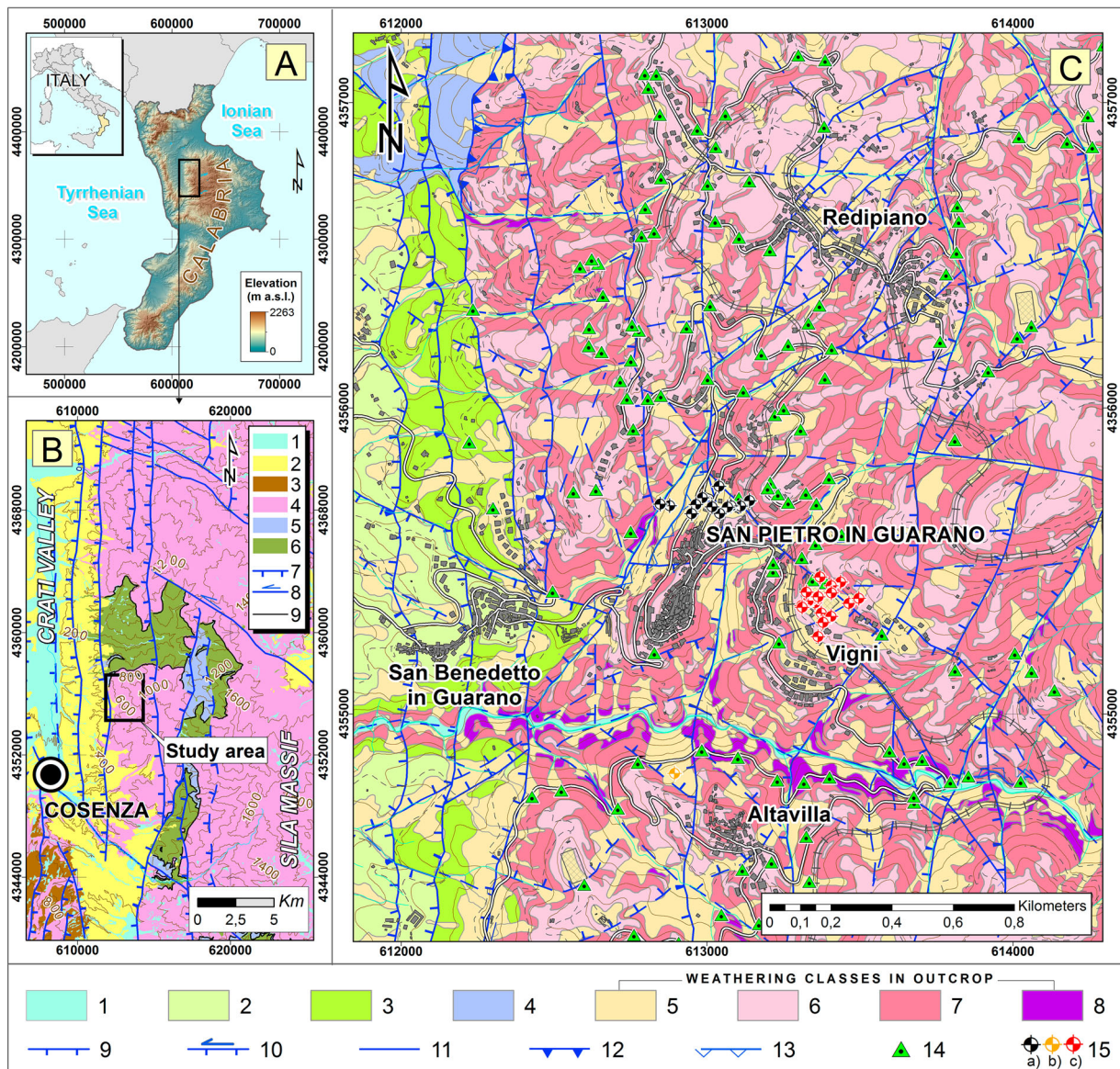

Figure 1. Geostructural setting of the study sector and area (Datum WGS84 Projection Transverse Mercator UTM, Zone 33 North). (A) Study sector. (B) Structural sketch of the western border of the Sila Massif (modified from Borrelli, Critelli, et al., 2015): (1) Holocene deposits; (2) Plio-Pleistocene deposits; (3) Miocene deposits; (4) Sila Unit (Paleozoic); (5) Castagna Unit (Paleozoic); (6) Bagni Unit (Paleozoic); (7) normal fault; (8) left lateral fault; (9) overthrust. (C) Geostructural and weathering grade map of the study area (from present study): (1) Holocene alluvial deposits; (2) clastic deposits composed by yellowish sands and sandstones (Lower Pleistocene); (3) conglomerates and breccias (Lower Pleistocene); (4) greenish-gray schists and milonitic paragneiss (Castagna Unit, Paleozoic); (5)–(8) biotite–garnet gneissic rocks, (5) class VI, (6) class V (completely weathered rocks); (7) class IV (highly weathered rocks); (8) class III (moderately weathered rocks); (9) normal fault; 13) strike-slip fault reactivated as normal fault; (11) undetermined fault; (12) overthrust; (13) thrust; (14) studied weathering profiles; (15) boreholes: (a) performed in the San Pietro in Guarano area, (b) performed in the Altavilla locality, (c) performed in the Vigni locality.

Arc) formed during the Paleogene, and overthrusted during the Miocene on the Apennine Carbonate Units (Bonardi et al., 1982). This massif consists of Paleozoic metamorphic (from low-to-high grade) and plutonic rocks (Figure 1(B)) belonging to the Sila Unit (Messina et al., 1994).

The Paleozoic crystalline rocks of the Sila Massif are discontinuously covered by unmetamorphosed Mesozoic to Cenozoic sedimentary rocks (e.g. Critelli, Muto, Tripodi, & Perri, 2011, 2013, 2017; Muto, Spina, Tripodi, Critelli, & Roda, 2014, 2015, 2017) (Figure 1(B)) and during the Neogene-Quaternary its margins were covered by terrigenous sedimentary successions (Fabbricatore, Robustelli, & Muto, 2014; Perri et al., 2012, 2014; Robustelli & Muto, 2017; Tansi et al., 2016; Zecchin, Praeg, Ceramicola, & Muto, 2015).

Referring to tectonics, the western margin of the Sila Massif (Figure 1(B)) is affected by high-angle Neogene-Quaternary fault systems (Matano & Tansi, 1994). The area experienced compressional and extensional tectonic events occurred during the northern Calabrian Arc development (Tansi, Muto, Critelli, & Iovine, 2007; Van Dijk et al., 2000).

The Quaternary tectonic uplift and the related deepening of the hydrographic network, along the western border of the Sila Massif, increased the relief energy, giving rise to steep slopes and deeply cut valleys in the bedrock and thus predisposing the slopes to the development of mass movements (Borrelli & Gullà, 2017 and references therein).

3. Method

The methodological approach followed to produce the Main Map of the study area (Figure 1(C)) includes three steps.

In the first step, geological investigations are carried out through aerial photo-interpretation and field surveys, to both investigate and verify the morphological evidence related to tectonics, as well as to identify faults and rock types. The geostructural setting of the study area was defined through both the interpretation of aerial color photographs (scale 1:15,000, acquired in 2001) and detailed field surveys (at 1:5000 scale) conducted during 2014. Geological surveys were used to identify the rock-type distribution on the area, and structural analysis (considering geometry, orientation and chronology of fault and fractures) was carried out to reveal the structural predisposition of slopes to landsliding.

In the second step, the study focused on the weathering grade field survey in order to produce a weathering grade map, following the procedure proposed by Borrelli, Coniglio, et al. (2015) and Borrelli, Critelli, et al. (2015). This procedure consists of the use of several criteria (e.g. rock color, discoloration processes, breaking samples by hands and hammer, the sound of the rock when struck by a geological hammer and the Schmidt Hammer tests) in order to distinguish six classes of weathering: class VI (residual and colluvial soils), class V (completely weathered rock), class IV (highly weathered rock), class III (moderately weathered rock), class II (slightly weathered rock) and class I (fresh rock).

During field surveys, 115 representative cutslopes (natural and artificial) have been examined in order to get information about the thickness and features of weathering profiles (Gullà & Matano, 1997). In addition, to investigate the characteristics of the weathering profiles in deep, the cutslope surveys were integrated by the analysis of 30 borehole logs (varying in depth from 10 to about 70 m) performed in the studied area during several geotechnical investigations carried out at different times (Cascini et al., 1992a, 1992b, 2006).

In the third step, a mass movement inventory map of the study area is produced on the basis of conventional (consolidated) methods (Conforti, Pascale, Pepe, Sdao, & Sole, 2013; Guzzetti et al., 2012), including (i) the visual interpretation of multi-temporal stereoscopic aerial photographs (1:33,000 scale, black-and-white, dated 1955 and 1990; 1:15,000 scale, color aerial photographs dated 2001) and (ii) geomorphological field surveys (carried out from September 2014 to March 2017). Field works were performed to validate inventory maps derived by the photo-interpretation (Brunsden, 1993). Landslide type and state of activity are established according to Cruden and Varnes (1996), and adopting geomorphological criteria based on field recognition and freshness of the topographic signatures typical of gravity-related landforms (Rib & Liang, 1978).

All mapped landslides have been grouped into three categories (shallow, medium-deep and deep-seated) according to the maximum thickness of the involved material, which was estimated on a geomorphological basis (e.g. Antronico, Borrelli, Coscarelli, & Gullà, 2015; Borrelli & Gullà, 2017; Gullà et al., 2017).

Finally, the Main Map is generated on a topographic base at 1:5000 scale (Technical Regional Map – CTR) and implemented in a Geographic Information System (GIS).

4. Results

4.1. Geological and structural setting of the study area

From a geological perspective, Paleozoic high-grade metamorphic rocks belonging to the Sila Unit and overthrusted on medium-grade metamorphic rocks, belonging to the Castagna Unit, widely outcrop in the study area (Messina et al., 1994) (Figure 1(C)).

The Castagna unit crops out only in the north-western edge of the examined area (Figure 1(C)). It is

composed mainly of greenish schists and paragneiss with mylonitic foliation and k feldspar porphyroclasts.

The metamorphic rocks belonging to the Sila Unit, widespread in the study area, are mainly composed of biotite–garnet migmatite gneiss (Figure 2(A,B)) and, locally, by biotite-rich and sillimanite gneiss (Figure 2 (C)). These rocks are often intruded by pegmatite and aplite dykes.

In the western portion of the study area (Figure 1 (C)), clastic deposits composed of conglomerates with crystalline pebble and boulders, brown to yellowish in color (Figure 2(D)) and medium-fine size yellowish sands (Figure 2(E)), outcrop.

Holocene colluvial deposits of variable thickness, derived from clastic slope-waste material, typically coarse-grained and immature, widespread in morphological hollows (Figure 2(F)) along the slopes and at the valley bottom.

From a tectonic viewpoint, structural analyses allowed us to recognize low-angle thrust (the oldest tectonic structures) that form duplex structures with pure compressive kinematics (Figure 3(A)). Oblique thrust ramps linked to the main thrusts show a horizontal component of movement (Figure 3(B)). The strike of these thrust varies between E-W and ENE, dipping to the south-east with an angle of inclination of average 20°.
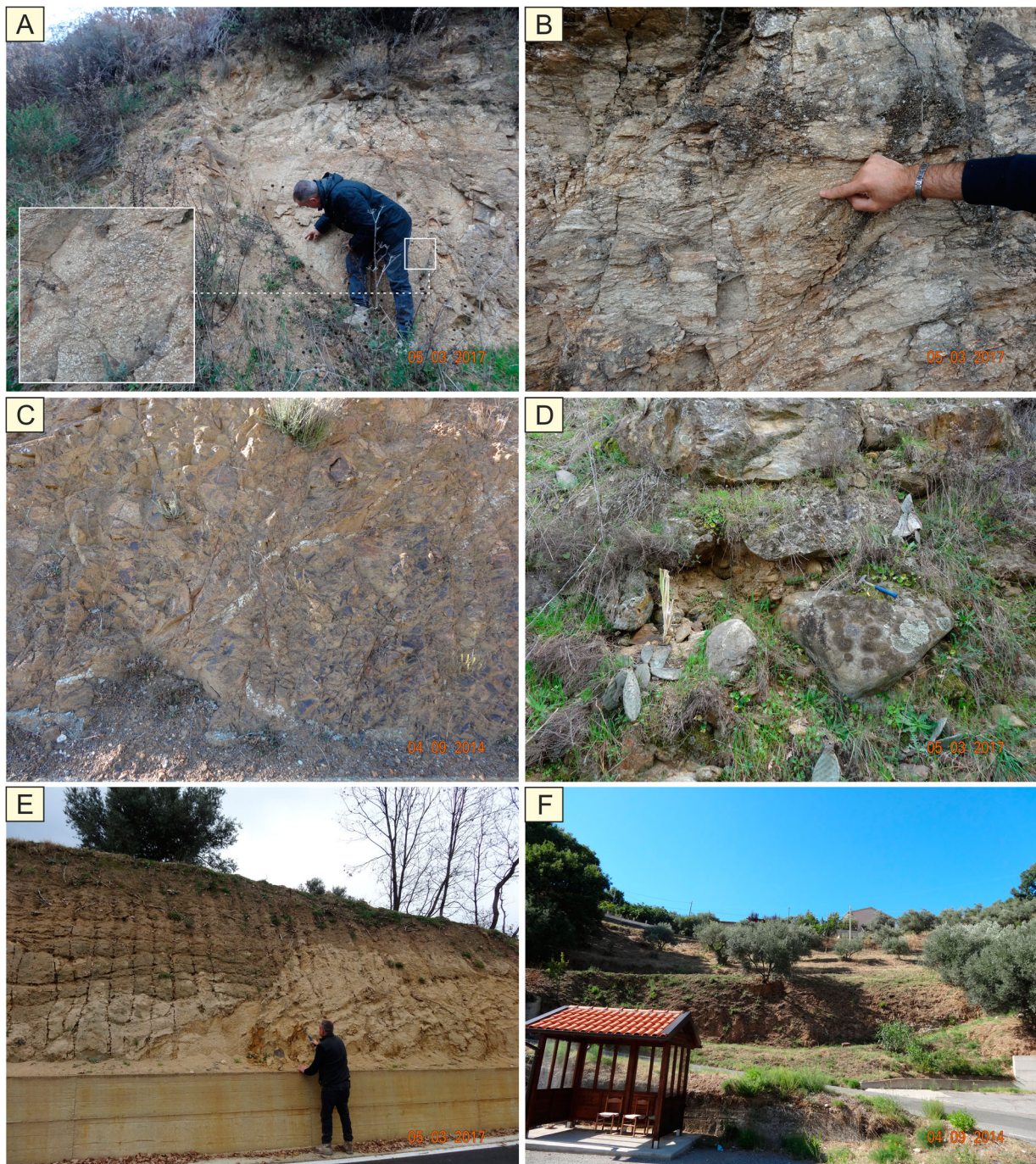

Figure 2. Lithologies outcropping in the study area: (A) biotite–garnet migmatite gneiss; (B) detail of the migmatite structure; (C) biotite-rich and sillimanite gneiss; (D) conglomerates; (E) sands and sandstones; (F) colluvial deposits.
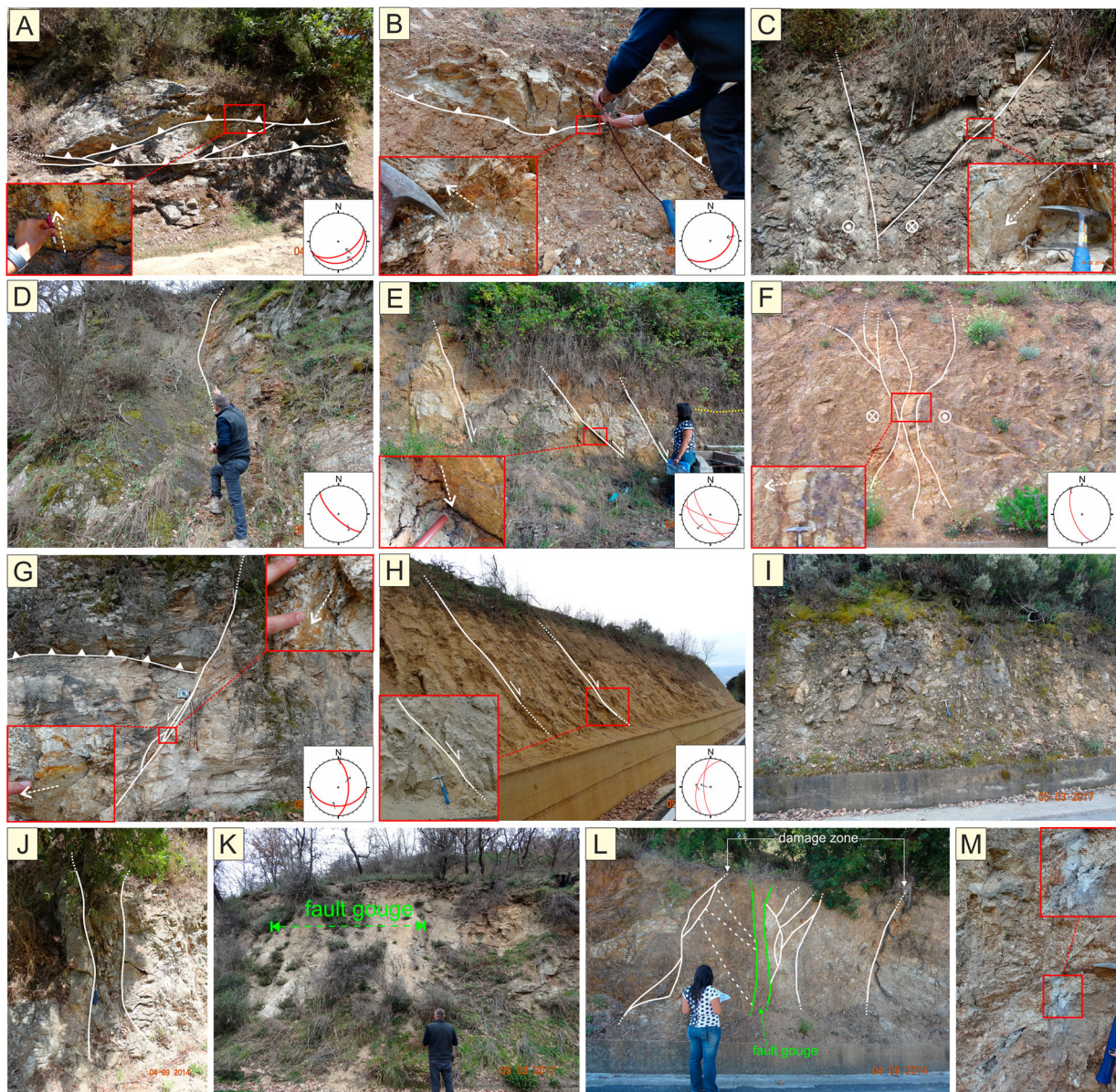
Figure 3. Examples of meso-faults surveyed in the study area: (A) low-angle thrust forming duplex structures; (B) oblique thrust ramp; (C), -(D) NW-SE left lateral strike-slip faults; (E) NW-SE normal faults; (F) N-S right-lateral fault; (G) N-S fault plane (superimposition of normal and left-lateral kinematics); (H) N-S dip-slip faults affecting Pleistocene sediments; (I), (J) fault breccias; (K), (L) fault gouge within fault damage zones; (M) clay-rich gouge along a fault plane.

The pre-Miocene duplex structures are offset by the main Neogene-Quaternary fault systems recognizable in the area, with NW-SE, NE-SW and N-S trends (Figure 1 (C)). These fault systems, according to Matano and Tansi (1994), are characterized by high-angle fault planes and by strike-slip, reverse and normal kinematics.

The NW trending faults crop out mainly along the Corno River valley (Figure 1(C)). The kinematics is typical of the regional NW transversal strike-slip fault system crosscutting the western border of the Sila Massif and in general the Calabrian belt (Tansi et al., 2007; Van Dijk et al., 2000) since the middle Miocene. Particularly, kinematics at the outcrop and mesoscopic scales consists in left lateral strike slips (Figures 3(C,D)) with pitch varying from 0° to 25°. The latest kinematics of this fault system consists in the normal reactivation of the earliest transcurrent faults (Figure 3(E)). In the

zone of off-lap or step-over of the strike-slip faults and in the bend of fault planes, transpressional geometry and kinematics are identified in the study area.

The NE-SW fault system outcrops close to the south of San Benedetto in Guarano and in the Redipiano zone (Figure 1(C)). It is represented by few sub-vertical, NW dipping fault planes with overprinted kinematic indicators and an inferred chronology that suggests right transcurrent or oblique-slip movements to which are associated dip-slip normal faults.

The N-S fault system is related to the last extensional phase of Calabria and is considered tectonically active (Spina, Tondi, & Mazzoli, 2011). The major N-S trending faults are characterized by fresh morphological evidence at macroscale (Figure 1(C)) and mesoscale. These structures are normal faults arranged into a westwards down-stepping system; fault planes are

Table 1. Field characterization of the weathering classes in the study area, based on geological observations and field tests.

Class	Rock mass	Rock material
Class III (moderately weathered rock)	The rock mass is moderately weathered (more than 70% of the outcrop); limited and isolated rock mass volumes may consist of highly to slightly weathered rock.	The rock material has mainly the following characteristics: pervasive change in color, although the color of the fresh rock can be present in places; original texture and microstructure of the fresh rock are well preserved; strength is comparable to that of the fresh rock (hard rock); rock makes an intermediate sound when it is struck by hammer; large pieces are hardly broken if it is struck by hammer head; the tip of a geological hammer produces a scratch on the rock surface. Ranges of the Schmidt Hammer rebound values: 24–41, mean 33.
Class IV (highly weathered rock)	The rock mass is highly weathered (more than 70% of the outcrop); limited and isolated rock mass volumes may consist of moderately to completely weathered rock.	The rock material has mainly the following characteristics: pervasive and complete change in color; original texture and microstructure of the fresh rock are still preserved; strength is substantially reduced (weak rock); rock makes an intermediate dull sound when it is struck by hammer; large pieces are easily broken if they are struck by hammer; large pieces do not slake in water; the tip of a geological hammer indents the rock superficially; knife edge produces a scratch on the surface of rock. Ranges of the Schmidt Hammer rebound values: 10–28, mean 20.
Class V (completely weathered rock)	The rock mass is completely weathered (saprolite) (more than 70% of the outcrop); limited and isolated rock mass volumes may consist of highly weathered rock or residual soil.	The rock material has mainly the following characteristics: complete change in color; original texture and microstructure of the fresh rock are present in relict form; strength is extremely reduced (soft rock or soil-like behavior); large pieces can be broken by hand and slake in water; the tip of a geological hammer indents the rock deeply; knife edge easily carves the surface of rock; gravel and sand fractions prevail. Ranges of the Schmidt Hammer rebound values: 0–17, mean 8.
Class VI (residual and colluvial soil)	The rock mass mainly consists of residual soils and colluvial/ detrital materials (more than 70% of the outcrop); limited and isolated portions may consist of moderately to highly weathered rock and/or saprolitic material.	The rock material has mainly the following characteristics: completely discolored; original texture and microstructure of the fresh rock are completely destroyed; soil-like behavior; large pieces can be easily broken by hand and crumbled by finger pressure into constituent grains. Residual soils (i.e. soils formed by weathering in place), rarely in outcrop and usually located at the top of the slopes, consist of mostly sand and silt size material with little or no clay fraction. Colluvial/detrital materials (i.e. locally transported detritus materials of soil horizons and parent materials of sloping terrains from the upper sections of the slopes through water erosion or landslides), usually located on slopes, foot slopes and in morphological depressions, mainly consist of sandy-silty to gravelly chaotic deposits, including moderately to highly weathered, centimetric to decimetric rock fragments.

generally characterized by clear kinematic indicators that, sometimes, show different slip-directions and pitch, also superimposed (Figure 3(G)). The relative chronology of the kinematic indicators suggests that right transcurrent movements and oblique transpressive slip postdate the last normal slip. The dip-slip faults affect both crystalline substrate and Pleistocene sediments (Figures 1(C) and 3(H)).

Generally, major faults are marked by high strained rocks (fault zones), including medium-to-coarse-grained cataclastic rocks (fault breccias, Figure 3(I,J)) fine grained cataclasite (fault gouge, Figures 3(K,L)) and clay-rich gouge (Figure 3(M)). Severe fracturing, which gave rise to polyhedric elements, with variable size from centimeter to several cubic meters, has favored the development and deepening of the weathering processes and the consequent physical–chemical decay of the gneissic rocks along the fault zones.

4.2. Weathering intensity

The weathering grade map (Figure 1(C) and Main Map) provides a general comprehensive overview of effects, intensity and spatial distribution of the weathering classes from classes VI to III. The qualitative characteristics and quantitative data of the outcropping weathering classes are summarized in Table 1. Referring to the spatial distribution of weathering grade in outcrop, class VI accounts for 31.2%, class V for about 29.0%, class IV for 37.5% and class III for 2.3%, whereas there is a total lack of classes II and I (respectively slightly weathered and fresh gneiss), which have been found only in some boreholes performed in the San Pietro in Guarano area (Figure 1).

In particular, class VI is randomly widespread along the slope from the top of the hill to the valley bottom (Figure 1), ranging in thickness from meters to decameters. Class VI consists of soil that was reworked and transported by slope processes (colluvial and slope debris deposits) and soil related to *in situ* weathering (residual soils). Slope debris (Figure 4(A)) are distributed along the slope and at the valley bottom; they are represented by disorganized deposits of sand and gravel, including moderately (class III) to highly (class IV) weathered decimetric rock fragments. Colluvial soils (Figure 4(B)) are found in morphological hollows (Figure 2(F)); they consist of sandy-silty chaotic deposits, including moderately to highly weathered

Figure 4. Examples of different classes of weathering in the gneissic rocks outcropping in the study area: (A) slope debris deposits (class VI); (B) colluvial soils (class VI); (C) residual soils (class VI); (D) completely weathered rock (class V); (E) highly weathered rock (class IV); (F) moderately weathered rock (class III).

centimetric rock fragments and subordinate organic fragments. Residual soils (Figure 4(C)), which are at least 2 m in thickness, outcrop exclusively at the top of the reliefs (e.g. Redipiano locality) and exhibit predominantly sandy and silty fractions. Results of the field surveys show that colluvial and slope debris deposits prevail over the residual one.

Class V (completely weathered rock) is mainly distributed (Figure 1(C)) in the summit portions of the slopes and reliefs – on flattened areas and present as relict strips at different altitudes – as well as at the base of the main structural slopes. The rock masses are completely weathered over more than 70% of the outcrop (Figure 4(D)), and the original rock strength is lost showing a soil-like behavior (the Schmidt Hammer values 0–17, mean 8); limited and isolated rock mass volumes can consist of highly weathered rock and residual soil (classes IV and VI, respectively).

Class IV (highly weathered rocks) outcrops extensively along the slopes, particularly at the middle-lower portions of reliefs (Figure 1(C)). These rock masses are highly weathered over more than 70% of the outcrop (Figure 4(E)) with limited and isolated volumes consisting of moderately to completely

weathered rock (classes III and V, respectively). The strength is substantially reduced with respect to the original unweathered rock (the Schmidt Hammer values 10–28, mean 20).

Class III (moderately weathered rocks) outcrops as strips of limited extension prevalently along the thalweg of the major stream incisions (e.g. Corno River and tributary streams), due to the deepening action of the watercourses (Figure 1(C)). The rock mass, which is moderately weathered over more than 70% of the outcrop (Figure 4(F)), is weaker than the fresh rock (the Schmidt Hammer values 24–41, mean 33); limited and isolated rock mass volumes can consist of highly and slightly weathered rock (classes IV and II, respectively).

The results of weathering grade surveys on the gneissic cutslopes, performed with the methodological approach proposed by Gullà and Matano (1997), allow one to identify characteristics and features of the outcropping weathering profiles.

The weathering profiles (whose location is shown in Figure 1(C)) are turned out particularly intense, as classes IV, V and VI are widespread, and complex (sensu) because of irregularities in the spatial distribution and thickness of weathered horizons which, due to the presence of structural discontinuities, generally do not have a wide lateral continuity (Figure 5(A,D)). Geometric relationships can be transitional (i.e. 'canonical' or 'normal/regular' sequence) or abrupt when controlled by joints/faults or rock structure (i.e. due to the compositional heterogeneity of the gneiss).

Along the middle-lower portions of slopes, generally in correspondence with stream incisions, cutslopes are mainly characterized by class III, with minor and/or local volumes of class IV (Figure 5(A)), because of erosion and deepening action of the watercourses.

Along the middle-upper portions of slopes, the cutslopes are mainly characterized by articulated geometric relationships between classes III, IV and V (Figure 5(B)). The cutslopes localized along the highest reliefs mainly show the presence of class V, with variable volumes of class IV, and thin covers of residual soil or colluvial soils (class VI) (Figure 5(C,D)).

The complexity of the outcropping weathering profiles is marked by the presence of tectonic structures (preferential pathways to the development of weathering and/or dislocation of different portions with a different weathering grade) and several pegmatite and aplite dikes (Figure 5(B,D)), mostly moderately weathered (class III).

The analysis of borehole logs (whose location is shown in Figure 1(C)) confirms the complexity of weathering profile in depth, highlighting articulated and complex geometric relationships between the various classes of weathering. In fact, along with some vertical profiles investigated by boreholes (Figure 5(E)), one can find out-of-sequence weathering horizons giving rise to a partial, or even complete inversion of the 'normal' weathering profile. In particular, the boreholes sited in San Pietro in Guarano and Altavilla (Figure 1(C)) are characterized by a prevalently vertical gradual transition from classes VI to II, the latter encountered at a variable depth between 5 and 40 m. On the contrary, in the boreholes collected in the Vigni locality (Figure 1(C)), the vertical transition occurs through the alternation of classes VI, V, IV and III, until the depth of 60 m (Figure 5(E)). These differences in terms of weathering profiles between the three investigated areas by boreholes are strongly related to their tectonic assemblage linked to fault displacements (Figure 1(C)).

4.3. Geomorphological setting and landslides

The mass movement inventory map (Figure 6 and Main Map) shows 174 landslides (of a different type, size, age and state of activity), with an average density of about 24 landslides/km^2. The inventory shows 125 slides (8 rock slides and 117 debris slides), 47 complex landslides (i.e. debris slide-debris flow), and 2 landslide zones affected by creep processes (Figure 6). The mapped landslides range in size from 136 to 273.868 m^2, totally affecting an area of about 1.5 km^2, namely the 20% of the whole study area. The analysis of the inventory map revealed that the 9% of the mapped landslides can be considered as active.

According to the maximum thickness of the involved material, all mapped landslides have been grouped into shallow, medium-deep and deep landslides (Figure 6 and Main Map).

Shallow landslides (e.g. slides and slide-flows less than 3 m deep, Figure 7(A,B)), in total 72 phenomena affecting an area of about 0.22 km^2, involve the soil cover (e.g. colluvial and residual soils) widespread along the slopes (Figure 6). From a geometrical perspective, these phenomena are from 5 to 40 m wide, and the total length depends on their evolution (once the phenomenon is triggered, it could either stop or develop into a debris flow). Characteristic features of these mass movements consist of little semicircular upper scarps and elongated bodies (up to 200 m) and accumulation zones, ending with U-shaped toes.

Medium-deep landslides (e.g. slides up to 30 m deep, Figure 7(C,D)), in total 99 phenomena affecting an area of about 0.85 km^2, mainly occurred within the morphological hollows (Figure 6) involving soil-like rocks (i.e. prevalently thick colluvial and residual covers and minor saprolitic soils); the width varies from approximately 50 to 150 m, and the length varies from approximately 60 to 370 m. Characteristic features of these mass movements consist of amphitheatre-shaped upper scarps, gently hummocky topography and ridges of accumulated material in the toe area, often causing the deviance of river channels.
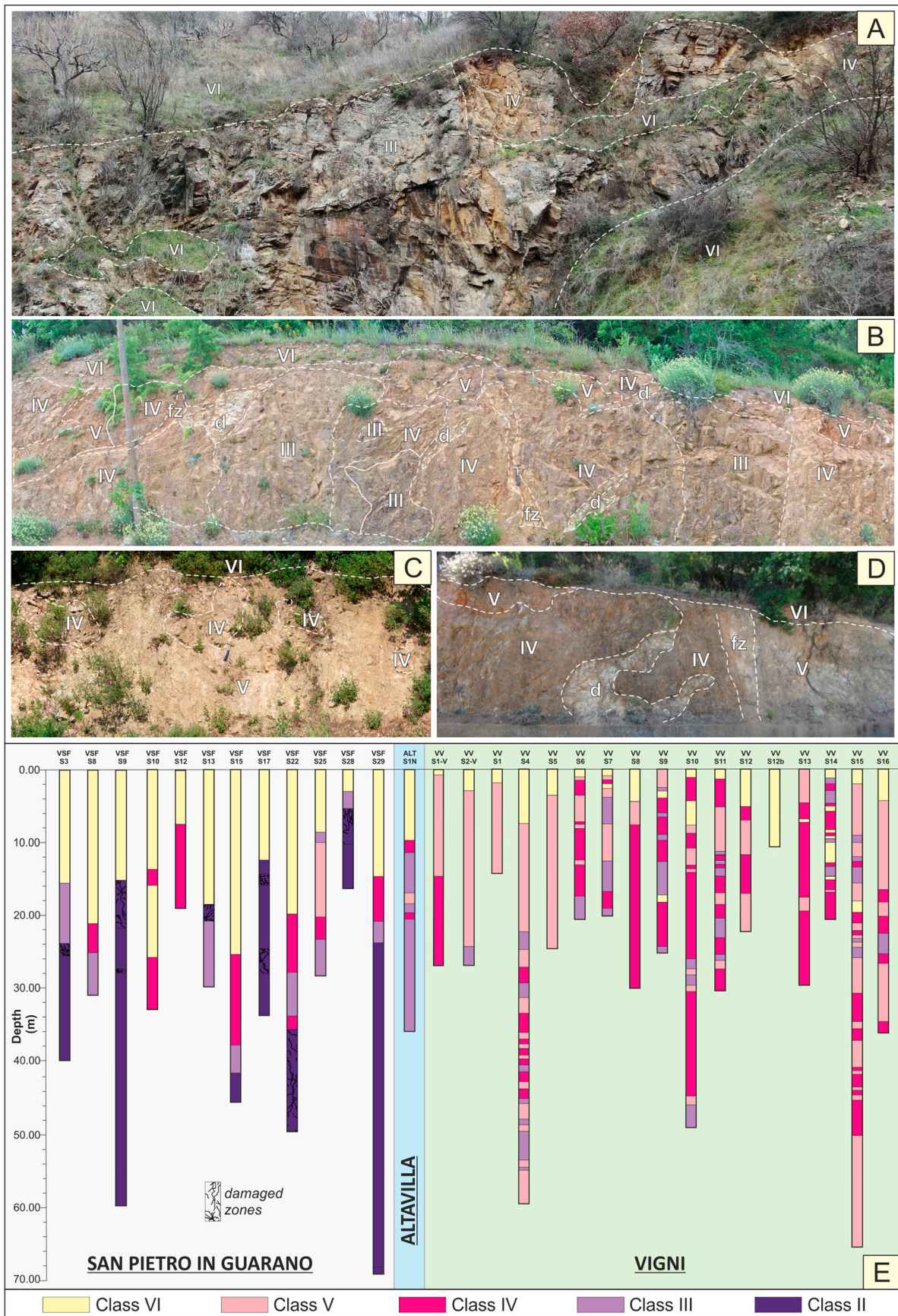
Figure 5. Examples of weathering profiles in the study area. (A) typical weathering profile outcropping in the middle-lower portions of the slopes, characterized by class III, with intercalations of class IV, overlain by colluvium and detrital slope deposits (class VI); (B) typical weathering profile outcropping along the middle-upper portions of the slopes, characterized by articulated geometric relationships between classes III, IV and V (d = dike of aplitic rock; fz = fault zone); (C), (D) typical weathering profiles outcropping along the highest reliefs, mainly showing the presence of class V, with variable volumes of class IV (d = dike of aplitic rock; fz = fault zone); (E) boreholes logs performed in the San Pietro in Guarano, Altavilla and Vigni localities (location in Figure 1(C)) reinterpreted in terms of weathering classes.
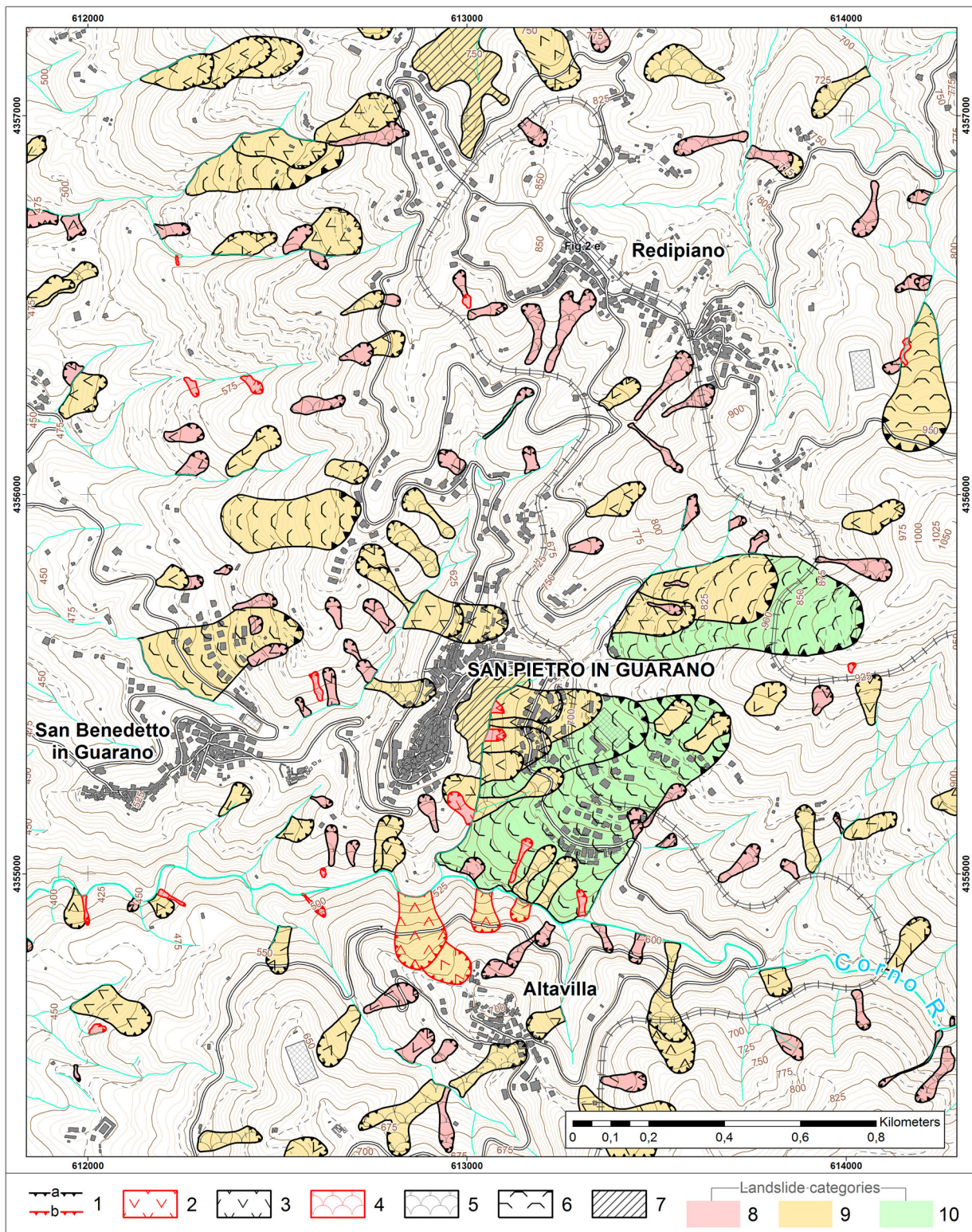
Figure 6. Landslide map of the study area: (1) landslide scarp ((a) dormant, (b) active); (2) active debris slide; (3) dormant debris slide; (4) active debris slide-debris flow (complex landslide); (5) dormant debris slide-debris flow (complex landslide); (6) dormant rock slide; (7) landslide zone affected by soil creep processes; (8) shallow landslide (less than 3 m deep); (9) medium-deep landslide (up to 30 m deep); (10) deep-seated landslide (deeper than 30 m).

Deep-seated landslides (e.g. large rock slides deeper than 30 m), which are the less widespread mass movements in the study area (in total three phenomena, affecting an area of about 0.42 km², Figure 6), involve significant thicknesses of variously weathered rocks of the gneissic basement (i.e. from classes VI to III). These landslides exhibit widths ranging from approximately 200 to 400 m and lengths ranging from approximately 400 to 800 m. Characteristic features of deep-seated landslides can be identified by aerial photographs showing their effects on the slope morphology, such as semicircular main scarps, counter

Figure 7. Types/categories of landslide affecting the study area: (A) active shallow debris slides; (B) active shallow complex landslide; (C) active medium-deep slide; (D) dormant medium-deep slide; (E) dormant rock slide (deep-seated landslide); (F) detail of the landslide flank coinciding with a NE-SW fault zone (G).

slopes, landslide terraces, irregular slope profiles, changes in the drainage network, and toe bulging (Cruden & Varnes, 1996; Hungr, Leroueil, & Picarelli, 2014; Varnes, 1978). Some of photo-interpreted landslide elements have been detected in the field, such as sheared rocks along the flanks of the landslide bodies (Figure 7(E–G)), coinciding with the main fault zones.

Finally, the data available from geological, geomorphological and weathering grade field surveys, integrated with the analyses of borehole logs, have been analyzed to summarize the relationships between each landslide category and weathering profiles; this synthesis allowed us to propose three simple block-models reported in Figure 8.

Shallow landslides (Figure 8(A)), mainly translational slides, prevalently involve class VI, and generally are triggered by extreme rainfall events (Gullà, 2014; Gullà et al., 2012; Terranova, Antronico, & Gullà, 2007).

Medium-deep landslides (Figure 8(B)), mainly classified as roto-translational slides, prevalently involve class VI. The extent of slip surfaces largely coincide with the contact between the upper regolith horizon (classes VI and V) and the weathered bedrock (classes IV and III), and they are generally triggered or reactivated by cumulative rainfall (Cascini & Versace, 1988; Gullà et al., 2009). According to Cascini, Gullà, and Sorbino (2006), due to landslide reactivation
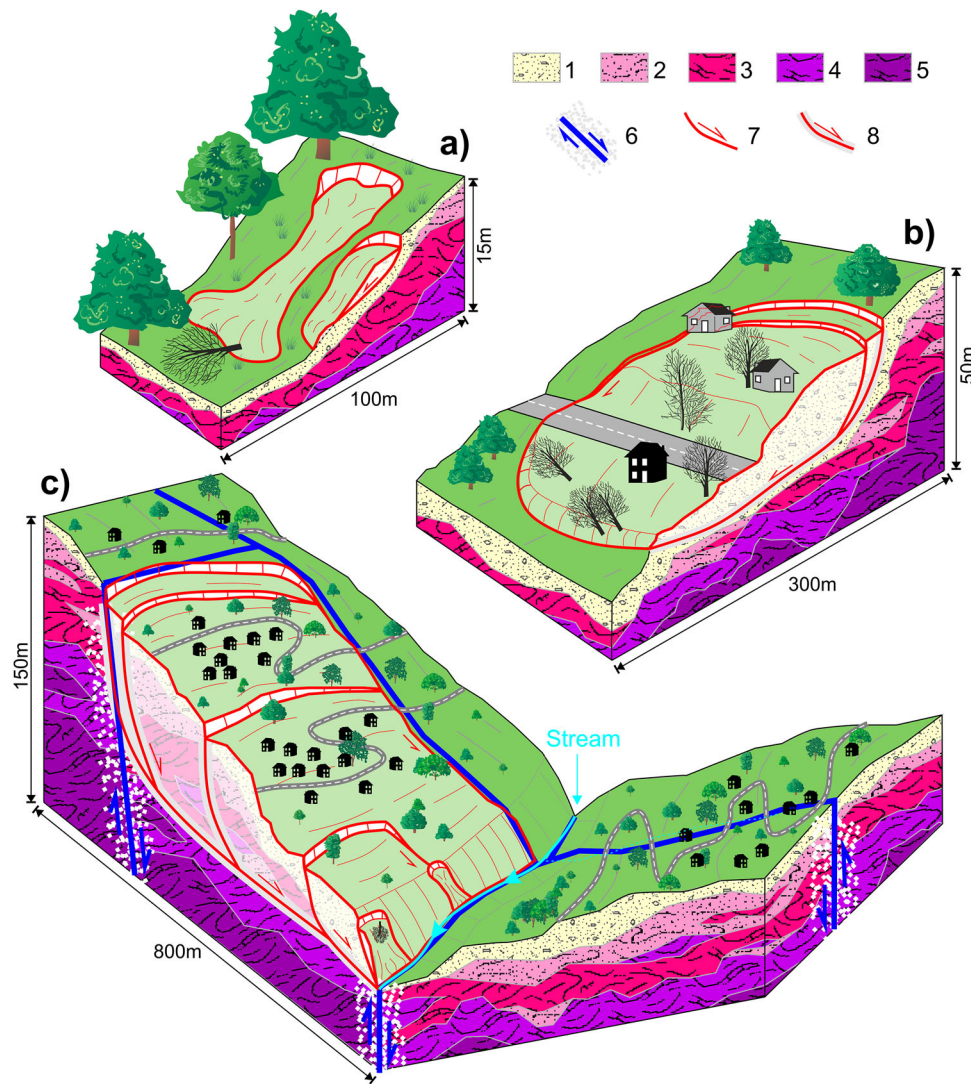
Figure 8. 3D block-models showing the relationships between landslide categories and weathering profiles in the study area: (A) shallow landslides; (B) medium-deep landslide; (C) deep-seated landslide. For explanations see the text. Note: (1) colluvial soils and slope debris deposits (class VI); (2) completely weathered rock (class V); (3) highly weathered rock (class IV); (4) moderately weathered rock (class III); (5) slightly weathered rock (class II); (6) fault plane with associated fault zone; (7) sliding surface; (8) sliding surface characterized by fine-grained materials produced by landslide reactivations (i.e. by cumulative displacements).

phases, we can find a higher presence of fine-grained soils in correspondence with slip surfaces.

Deep-seated landslides (Figure 8(C)), mainly translational rock slides, involve considerable thicknesses of variously weathered rocks (i.e. classes VI, V, IV and III). Sliding surfaces are located within classes IV to III (driven by foliation planes or low-angle thrust surfaces) and, generally, the remobilization can be achieved when prolonged and intense rainfall and snowmelt events occur (Gullà, 2014). For this landslide category, the tectonic control plays an important role in its development and evolution in the space and time (i.e. fault-related landslides).

5. Conclusions

The paper presented a detailed thematic map (Main Map) of the San Pietro in Guarano area (about 7.5 km², located along the western border of the Sila Massif (Calabria, Italy).

This area is a representative case study, where lithology (i.e. weathered gneissic rocks), tectonic setting, high relief and steep slopes predispose to the development of widespread landslides.

The Main Map (performed at 1:5000 scale) is the result of an integrated and interdisciplinary study based on (i) analysis and interpretation of aerial photographs at different times and scales; (ii) geostructural and multi-temporal geomorphological field surveys; and (iii) field investigations and mapping of weathering grade in outcrop, coupled with the analysis of both weathering profiles on cutslopes and geotechnical boreholes logs.

The Main Map provides a general and comprehensive overview of effects, intensity, and spatial distribution of weathering classes and associated tectonic constraints. The analysis of weathering profiles on cutslopes and the characteristics of weathering profiles in depth (investigated by geotechnical boreholes logs)

allow us to evaluate that the weathering front propagates downward until 60 m. The typical weathering profiles are generally complex and characterized by irregularities in the spatial distribution and thickness of weathered classes. These aspects strongly control the development of landslides in the study area.

The analysis of the acquired data enables us to identify one simple block model for each landslide category. The three proposed conceptual models, summarizing the relationships between landslide categories and weathering profiles, can also be considered representative of the western geo-environmental context of the Sila Massif and exportable to other geotectonic settings with similar weathering profiles.

The Main Map can represent a useful tool for authorities in charge of land-use planning and can profitably concur to typify landslides, and to pursue quantitative landslide risk assessment.

Software

The Main Map and related layout (Figures 1 and 6) were carried out using the ESRI ArcGIS 10.0. Corel Draw X6 was used for compiling Figures 2–5, 7 and 8.

Acknowledgements

Disclosure statement

No potential conflict of interest was reported by the authors.

ORCID

Luigi Borrelli http://orcid.org/0000-0003-2833-788X
Giovanni Gullà http://orcid.org/0000-0003-1165-4782

References

Antronico, L., Borrelli, L., Coscarelli, R., & Gullà, G. (2015). Time evolution of landslide damages to buildings: The case study of Lungro (Calabria, southern Italy). *Bulletin of Engineering Geology and the Environment*, 74, 47–59.

Bonardi, G., Cello, G., Perrone, V., Tortorici, L., Turco, E., & Zuppetta, A. (1982). The evolution of the northern sector of the Calabria-Peloritani Arc in a semiquantitative palinspastic restoration. *Bollettino della Società Geologica Italiana*, 101, 259–274.

Borrelli, L., Ciurleo, M., & Gullà, G. (2018). Shallow landslide susceptibility assessment in granitic rocks using GIS-based statistical methods: The contribution of the weathering grade map. *Landslides*, 1–16. doi:10.1007/s10346-018-0947-7

Borrelli, L., Coniglio, S., Critelli, S., La Barbera, A., & Gullà, G. (2015). Weathering grade in granitoid rocks: The San Giovanni in Fiore area (Calabria, Italy). *Journal of Maps*, 12(2), 260–275.

Borrelli, L., Critelli, S., Gullà, G., & Muto, F. (2015). Weathering grade and geotectonics of the western-central Mucone River basin (Calabria, Italy). *Journal of Maps*, 11, 606–624.

Borrelli, L., Greco, R., & Gullà, G. (2007). Weathering grade of rock masses as a predisposing factor to slope instabilities: Reconnaissance and control procedure. *Geomorphology*, 87, 158–175.

Borrelli, L., & Gullà, G. (2017). Tectonic constraints on a deep-seated rock slide in weathered crystalline rocks. *Geomorphology*, 290, 288–316.

Borrelli, L., Perri, F., Critelli, S., & Gullà, G. (2012). Mineropetrographical features of weathering profiles in Calabria, southern Italy. *Catena*, 92, 196–207.

Borrelli, L., Perri, F., Critelli, S., & Gullà, G. (2014). Characterization of granitoid and gneissic weathering profiles of the Mucone River basin (Calabria, southern Italy). *Catena*, 113, 325–340.

Brunsden, D. (1993). Mass movements; the research frontier and beyond: A geomorphological approach. *Geomorphology*, 7, 85–128.

Calcaterra, D., & Parise, M. (2005). Landslide types and their relationships with weathering in a Calabrian basin, southern Italy. *Bulletin of Engineering Geology and the Environment*, 64, 193–207.

Calcaterra, D., & Parise, M. (2010). Weathering in the crystalline rocks of Calabria, Italy, and relationships to landslides. In D. Calcaterra & M. Parise (Eds.), *Weathering as a predisposing factor to slope movements* (pp. 105–130. Geological Society of London, 23. Engineering Geology Special Publication.

Cascini, L., Ciurleo, M., & Di Nocera, S. (2017). Soil depth reconstruction for the assessment of the susceptibility to shallow landslides in fine-grained slopes. *Landslides*, 14 (2), 459–471.

Cascini, L., Critelli, S., Di Nocera, S., Gullà, G., & Matano, F. (1992a). Grado di alterazione e franosità negli gneiss del Massiccio silano: L'area di S. *Pietro in Guarano (CS). Geologia Applicata e Idrogeologia*, 27, 49–76.

Cascini, L., Critelli, S., Di Nocera, S., Gullà, G., & Matano, F. (1992b). *A methodological approach to landslide hazard assessment: A case history*. Proceedings of the 6th International Symposium on Landslides, Christchurch, 10–14 February 1992 (Vol. 2, pp. 899–904).

Cascini, L., Critelli, S., Di Nocera, S., Gullà, G., & Matano, F. (1994). *Weathering and landsliding in Sila Massif gneiss (Northern Calabria, Italy)*. Proceedings of the 7th International IAEG Congress (pp. 1613–1622), Lisboa, Portugal.

Cascini, L., & Gullà, G. (1993). Caratterizzazione fisico-meccanica dei terreni prodotti dall'alterazione di rocce gneissiche. *Rivista Italiana di Geotecnica*, 2, 125–147.

Cascini, L., Gullà, G., & Sorbino, G. (2006). Groundwater modelling of a weathered gneissic cover. *Canadian Geotechnical Journal*, 43, 1153–1166.

Cascini, L., & Versace, P. (1988). *Relationship between rainfall and landslide in a gneissic cover*. Proceedings of the 5th International Symposium on Landslides, Lausanne (pp. 565–570).

Chigira, M., & Ito, E. (1999). Characteristic weathering profiles as basic causes of shallow landslides. In N. Yagi, T. Yamagami, & J. C. Jiang (Eds.), *Slope stability engineering* (pp. 1145–1150). Rotterdam: Balkema.

Chiu, C. F., & Charles, W. W. N. (2014). Relationships between chemical weathering indices and physical and mechanical properties of decomposed granite. *Engineering Geology*, 179, 76–89.

Ciurleo, M., Cascini, L., & Calvello, M. (2017). A comparison of statistical and deterministic methods for shallow landslide susceptibility zoning in clayey soils. *Engineering Geology*, 223, 71–81.

Conforti, M., Pascale, S., Pepe, M., Sdao, F., & Sole, A. (2013). Denudation processes and landforms map of the Camastra River catchment (Basilicata–South Italy). *Journal of Maps*, 9, 444–455.

Critelli, S., Di Nocera, S., & Le Pera, E. (1991). Approccio metodologico per la valutazione petrografica del grado di alterazione degli gneiss del Massiccio Silano – Calabria settentrionale. *Geologia Applicata e Idrogeologia*, 26, 41–70.

Critelli, S., Muto, F., Perri, F., & Tripodi, V. (2017). Interpreting provenance relations from sandstone detrital modes, southern Italy foreland region: Stratigraphic record of the Miocene tectonic evolution. *Marine and Petroleum Geology*, 87, 47–59.

Critelli, S., Muto, F., Tripodi, V., & Perri, F. (2011). Relationships between lithospheric flexure, thrust tectonics and stratigraphic sequences in foreland setting: The southern Apennines foreland basin system, Italy. In U. Schattner (Ed.), *New frontiers in tectonic research—at the midst of plate convergence* (pp. 121–170). Rijeka: InTech.

Critelli, S., Muto, F., Tripodi, V., & Perri, F. (2013). Link between thrust tectonics and sedimentation processes of stratigraphic sequences from the southern Apennines foreland basin system, Italy. *Rendiconti Online della Società Geologica Italiana*, 25, 21–42.

Cruden, D. M., & Varnes, D. J. (1996). Landslide types and processes. In A. K.Turner & R. L. Schuster (Eds.), *Landslides investigation and mitigation. Transportation research board* (pp. 36–75). US National Research Council. Special Report 247, Washington, DC.

Fabbricatore, D., Robustelli, G., & Muto, F. (2014). Facies analysis and depositional architecture of shelf-type deltas in the Crati Basin (Calabrian Arc, south Italy). *Italian Journal of Geosciences*, 133, 131–148.

Gullà, G. (2014). Field monitoring in sample sites: Hydrological response of slopes with reference to widespread landslide events. *Procedia Earth and Planetary Science*, 9, 44–53.

Gullà, G., Aceto, L., & Borrelli, L. (2012). Terreni di alterazione da rocce cristalline. *Rendiconti Online della Società Geologica Italiana*, 21, 548–550.

Gullà, G., Antronico, L., Borrelli, L., Caloiero, T., Coscarelli, R., Iovine, G., … Terranova, O. (2009). Indicazioni conoscitive e metodologiche connesse all'evento di dissesto idrogeologico dell'autunno-inverno 2008–2009 in Calabria. *Geologi Calabria*, 10, 4–21.

Gullà, G., Borrelli, L., & Greco, R. (2004). *Weathering of rock-mass as possible characterizing factor of predisposition to slope instabilities*. Proceedings of the 9th international symposium on landslides (pp. 103–108), Rio de Janeiro, Brazil.

Gullà, G., & Matano, F. (1997). *Surveys of weathering profile on gneiss cutslopes in Northern Calabria, Italy*. Proceedings of the 8th International Symposium on Engineering Geology and the Environment (pp. 133–138), Athens, Greece.

Gullà, G., Peduto, D., Borrelli, L., Antronico, L., & Fornaro, G. (2017). Geometric and kinematic characterization of landslides affecting urban areas: The Lungro case study (Calabria, Southern Italy). *Landslides*, 14, 171–188.

Guzzetta, G. (1974). Ancient tropical weathering in Calabria. *Nature*, 251, 302–303.

Guzzetti, F., Mondini, A. C., Cardinali, M., Fiorucci, F., Santangelo, M., & Chang, K. T. (2012). Landslide inventory maps: New tools for an old problem. *Earth-Science Reviews*, 112, 42–66.

Hungr, O., Leroueil, S., & Picarelli, L. (2014). The Varnes classification of landslide types, an update. *Landslides*, 11, 167–194.

Ietto, F., Perri, F., & Cella, F. (2018). Weathering characterization for landslides modeling in granitoid rock masses of the Capo Vaticano promontory (Calabria, Italy). *Landslides*, 15, 43–62.

Le Pera, E., Critelli, S., & Sorriso-Valvo, M. (2001). Weathering of gneiss in Calabria, southern Italy. *Catena*, 42, 1–15.

Le Pera, E., & Sorriso-Valvo, M. (2000). Weathering and morphogenesis in a Mediterranean climate, Calabria, Italy. *Geomorphology*, 34, 251–270.

Matano, F., & Di Nocera, S. (1999). Weathering patterns in the Sila Massif (northern Calabria, Italy). *Journal of Quaternary Science*, 12, 141–148.

Matano, F., & Tansi, C. (1994). Influenza delle strutture tettoniche sul profilo di alterazione e sulla franosità negli gneiss dell'area di San Pietro in Guarano (Calabria Settentrionale). *Geologica Romana*, 30, 361–370.

Messina, A., Russo, S., Borghi, A., Colonna, V., Compagnoni, R., Caggianelli, A., … Piccarreta, G. (1994). Il Massiccio della Sila Settore settentrionale dell'Arco Calabro-Peloritano. *Bollettino della Società Geologica Italiana*, 113, 539–586.

Muto, F., Critelli, S., Robustelli, G., Tripodi, V., Zecchin, M., Fabbricatore, D., & Perri, F. (2015). A Neogene-Quaternary Geotraverse within the Northern Calabria Arc from the foreland peri-Ionian margin to the backarc Tyrrhenian margin. *Geological Field Trips*, 7(2.2), 65.

Muto, F., Spina, V., Tripodi, V., Critelli, S., & Roda, C. (2014). Neogene tectonostratigraphic evolution of allochthonous terranes in the eastern Calabrian foreland (southern Italy). *Italian Journal of Geosciences*, 133, 455–473.

Muto, F., Tripodi, V., Chiarella, D., Lucà, F., & Critelli, S. (2017). Tectono-stratigraphic architecture of the Ionian piedmont between the Arso stream and Nicà river catchments (Calabria, Southern Italy). *Journal of Maps*, 13, 332–341.

Pellegrino, A., & Prestininzi, A. (2007). Impact of weathering on the geomechanical properties of rocks along thermal–metamorphic contact belts and morpho-evolutionary processes: The deep-seated gravitational slope deformations of Mt. Granieri–Salincriti (Calabria– Italy). *Geomorphology*, 87, 176–195.

Perri, F., Borrelli, L., Critelli, S., & Gullà, G. (2014). Chemical and minero-petrographic features of Plio-Pleistocene fine-grained sediments in Calabria (southern Italy). *Italian Journal of Geosciences*, 133, 101–115.

Perri, F., Critelli, S., Dominici, R., Muto, F., Tripodi, V., & Ceramicola, S. (2012). Provenance and accommodation pathways of late Quaternary sediments in the deep-water northern Ionian Basin, southern Italy. *Sedimentary Geology*, 280, 244–259.

Regmi, A. D., Yoshida, K., Dhital, M. R., & Pradhan, B. (2014). Weathering and mineralogical variation in gneissic rocks and their effect in Sangrumba Landslide, East Nepal. *Environmental Earth Sciences*, 71, 2711–2727.

Rib, H. T., & Liang, T. (1978). Recognition and identification. In R. L. Schuster & R. J. Krizek (Eds.), *Landslide analysis and control. Transportation research board special report 176* (pp. 34–80). Washington, DC: National Academy of Sciences.

Robustelli, G., & Muto, F. (2017). The Crati River Basin. Geomorphological and stratigraphical data for the Plio-Quaternary evolution of northern Calabria, South Apennines, Italy. *Geologica Carpathica*, *68*(1), 68–79.

Scarciglia, F., Critelli, S., Borrelli, L., Coniglio, S., Muto, F., & Perri, F. (2016). Weathering profiles in granitoid rocks of the Sila Massif uplands, Calabria, southern Italy: New insights into their formation processes and rates. *Sedimentary Geology*, *336*, 46–67.

Scarciglia, F., Le Pera, E., & Critelli, S. (2005). Weathering and pedogenesis in the Sila Grande Massif (Calabria, South Italy): from field scale to micromorphology. *Catena*, *61*, 1–29.

Spina, V., Tondi, E., & Mazzoli, S. (2011). Complex basin development in a wrench-dominated back-arc area: Tectonic evolution of the Crati Basin, Calabria, Italy. *Journal of Geodynamics*, *51*, 90–109.

Tansi, C., Folino Gallo, M., Muto, F., Perrotta, P., Russo, L., & Critelli, S. (2016). Seismotectonics and landslides of the Crati Graben (Calabrian Arc, Southern Italy). *Journal of Maps*, *12*, 363–372.

Tansi, C., Muto, F., Critelli, S., & Iovine, G. (2007). Neogene-Quaternary strike-slip tectonics in the central Calabrian Arc (Southern Italy). *Journal of Geodynamics*, *43*, 393–414.

Terranova, O., Antronico, L., & Gullà, G. (2007). Landslide triggering scenarios in homogeneous geological contexts: The area surrounding Acri (Calabria, Italy). *Geomorphology*, *87*, 250–267.

Van Dijk, J. P., Bello, M., Brancaleoni, G. P., Cantarella, G., Costa, V., Frixa, A., … Zerilli, A. (2000). A regional structural model for the northern sector of the Calabria Arc (Southern Italy). *Tectonophysics*, *324*, 267–320.

Varnes, D. J. (1978). Slope movement types and processes. In R. L. Schuster & R. J. Krizek (Eds.), *Special report 176: Landslides, analysis and control* (pp. 11–33). Washington, DC: Transportation and Road Research Board, National Academy of Science.

Whalley, W. B., & Turkington, A. V. (2001). Weathering and geomorphology. *Geomorphology*, *41*, 1–3.

Zecchin, M., Praeg, D., Ceramicola, S., & Muto, F. (2015). Onshore to offshore correlation of regional unconformities in the Plio-Pleistocene sedimentary successions of the Calabrian Arc (central Mediterranean). *Earth-Science Reviews*, *142*, 60–78.